

Published in final edited form as:

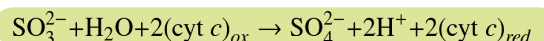
*Chem Biodivers.* 2012 September ; 9(9): 1621–1634. doi:10.1002/cbdv.201200010.

## C12010. Kinetic and Thermodynamic Effects of Mutations of Human Sulfite Oxidase

Asha Rajapakse\*, Gordon Tollin, and John H. Enemark\*

Department of Chemistry and Biochemistry, The University of Arizona, 1306 E. University Blvd., Tucson, Arizona 85721-0041 U.S.A.

Sulfite oxidizing enzymes, which catalyze the oxidation of sulfite to sulfate, can be categorized into two classes based on their ability to transfer electrons to molecular oxygen: the sulfite oxidases (SO) found in animals and plants, and the sulfite dehydrogenases (SDH) found in bacteria. Animal SO is localized in mitochondria and utilizes cytochrome *c* (cyt *c*) as the physiological terminal electron acceptor (eq. 1), while for plant SO located in peroxisomes, molecular oxygen serves as the terminal electron acceptor.



Eq 1. also represents the final step in the oxidative degradation of the sulfur containing amino acids cysteine and methionine in humans. The detoxification of exogenously supplied sulfite and sulfur dioxide is also catalyzed by SO. The loss of ability to oxidize sulfite can be due to either a defect in the biosynthetic pathway of the molybdenum cofactor (Moco) or point mutations in the *sox* gene itself, [1] resulting in sulfite oxidase deficiency. The biochemical basis of the pathology of sulfite oxidase deficiency is not yet known. The recent advancements in the knowledge of the biosynthetic pathway of the molybdenum cofactor has made possible the first clinical treatment of SO deficiency in 2010 [2].

All SO, except plant SO, possess two redox centers located in the Mo and heme domains. The relative arrangement of these two domains in the solid state in animal SO was established by the X-ray structure of native chicken SO (cSO). In this homodimeric protein, each subunit houses a small N-terminus cyt *b*<sub>5</sub> heme, a large central Mo domain, and a large C-terminus interface domain. No crystal structure is yet available for human SO (hSO), and presently the structure of the highly homologous native cSO serves as a structural template for analyzing hSO [3]. The Mo and the heme domains in each subunit are linked by a flexible peptide loop of 13 amino acid residues. Two oxo groups and three sulfur atoms, one from the C185 residue and two from the pyranopterindithiolate (molybdopterin), coordinate the Mo atom. As with many multi-redox enzymes, intramolecular electron transfer (IET) between the Mo and the Fe centers are pivotal to enzymatic turnover. The rates of IET in SO have been studied intensively over many years, primarily by our group [4–9]. This review focuses on recent advances in understanding IET in hSO and the implications of the results for human SO deficiency.

### Proposed catalytic mechanism for SO

The catalytic mechanism proposed for SO is summarized in Fig. 1 [10, 11]. The fully oxidized Fe(III)/Mo(VI) resting state is shown in **1**; sulfite (substrate) reacts with the

\*Phone: 520-621-2245 Fax: 520-626-8065 rajapaks@email.arizona.edu and jenemark@email.arizona.edu.

Mo(VI) site to generate **2** (Fe(III)/Mo(IV)) and produce sulfate (product); rapid intramolecular electron transfer (IET 1) produces **3** (Fe(II)/Mo(V)) which is detected by the change in the heme spectrum and by the appearance of a Mo(V) EPR signal. Reaction of **3** with oxidized cyt *c* generates **4** (Fe(III)/Mo(V)) which undergoes IET 2 to generate **5** (Fe(II)/Mo(VI)). Rajagopalan [10] originally proposed that **5** would react with excess sulfite to generate **6** (Fe(II)/Mo(IV)), which would then react with oxidized cyt *c* to regenerate **2** and continue the catalytic cycle. More recent proposals [12, 13] have **5** reacting with oxidized cyt *c* to regenerate the fully oxidized resting state, **1**, for continued catalysis.

In the catalytic mechanism, the conversion of **1** to **3** is termed the reductive half-reaction. The oxidative half-reaction involves two one-electron transfers to cyt *c* to yield oxidized SO (**1**) and two molecules of reduced cyt *c*. The oxidative half-reaction also includes the IET 2 step (**4** → **5**). The kinetics of the reductive and oxidative half-reactions can be determined by stopped-flow methods by monitoring the reduction of the *b*-type heme and cyt *c*, respectively. Stopped-flow studies by Rajagopalan *et al.* on the truncated Mo domain and full-length hSO gave evidence that reduction of the Mo center is fast, indicating that this step (**1** to **3**) is not the rate-limiting step in the catalytic cycle [14, 15]. Thus, the rate limiting step in the overall *wt* hSO catalytic cycle is as yet unknown. However, various studies on hSO variants have revealed that IET can become the rate limiting step in catalysis, as will be discussed in detail later.

### IET in hSO

Both mechanisms of Fig. 1 involve two IET steps, and IET 2, which involves **4** and **5**, and IET 1 involving **2** and **3**, are necessary for the catalytic turnover. Steady-state kinetics studies give  $k_{\text{cat}}$  for the overall reaction, and several approaches have been used to probe the individual steps of the cycle of Fig. 1. Stopped-flow kinetics studies of the reaction of sulfite with oxidized SO (**1**) give the overall rate of conversion **1** to **3** [16], but cannot separate the postulated IET 1 step. Laser flash photolysis (LFP) can be used to convert **1** to **5**, and the rate of the IET 2 step to generate **4** can be followed by monitoring the change in absorbance of the  $b_5$ -type heme [8]. LFP experiments can be performed anaerobically in solutions containing 5-deazariboflavin (DRF) and freshly prepared semicarbazide or EDTA ( $\text{AH}_2$ ) as a sacrificial reductant. The DRF radicals generated *in situ* with a laser pulse will rapidly reduce the Fe(III) heme center in SO by one electron (see dotted arrow in Fig. 1, Steps **1** to **5**), followed by intramolecular equilibration between the redox centers (**5** and **4**). A typical transient kinetic trace obtained from a LFP experiment is shown in Fig. 2. Note that the laser flash photolysis technique follows the IET process in the reverse direction of the enzymatic turnover. The methodologies used to obtain rate and equilibrium constants for IET in SO have been described previously [17]. The observed rate constant ( $k_{\text{et}}$ ) reflects the sum of the forward ( $k_f$ ) and reverse ( $k_r$ ) rate constants for electron transfer independent of the direction in which the redox equilibrium is shifted experimentally. The IET rate constants measured using this technique for selected hSO mutants are listed in Table 1. Several of these mutants will be discussed in detail later. In addition to these kinetic parameters, this technique also allows measurement of the equilibrium constant ( $K_{\text{eq}}$ ) for the reaction (**4**  $\rightleftharpoons$  **5**).

According to simple Marcus theory considerations [18], the primary factors in determining IET rates are the distance between the two cofactors and their mutual orientation in the intervening medium, the thermodynamic driving force, and the reorganization energy. In the case of proteins, to this must be added the rates of any conformational steps involved in bringing the two redox centers into mutual contact [19]. The observed IET rate constants for *wt* hSO are much faster than expected for the large distance between the two redox centers (ca. 32 Å) observed for the resting state in the crystallographic structure of cSO and for the small difference in reduction potentials determined for these two cofactors [20, 21]. To

explain this discrepancy, it has been proposed that in solution the negatively charged cytochrome *b*<sub>5</sub> domain is reoriented towards the positively charged Mo active site to reduce the Mo-Fe distance and thereby achieve rapid IET, and that this conformational step is rate-limiting for the IET process [17, 22–24]. Both experimental and theoretical models support the idea of the heme domain docking at the positively charged Mo active site [17, 23]. Extensive flash photolysis studies on native cSO and wild-type recombinant hSO have shown that the IET 2 rate constants depend on solution viscosity [8, 23, 25], sulfate concentrations [17, 26, 27], and pH [17, 27, 28]. However, it is important to note that IET is *not* rate-limiting for overall catalytic turnover in *wt* cSO and hSO.

Sulfite oxidation at the Mo active site involves three major steps: binding of sulfite, electron transfer to the heme *b*<sub>5</sub>, and product release. The positively charged Mo active site pocket offers an ideal environment for binding of anionic sulfite. However, the sequence of the steps following substrate binding, i.e. sulfate release and IET, is not completely understood. Simultaneous association of sulfite and the heme of the cytochrome *b*<sub>5</sub> domain with the Mo center would be expected to be a sterically and energetically unfavorable process. Indeed, previous studies have shown that anion binding to SO greatly decreases IET [17, 23] and that anions show mixed-noncompetitive patterns of inhibition on catalysis [29, 30]. Recent IET studies on several aromatic hSO mutants shed some light into possible alternative electron transfer pathways, which will be discussed later.

### Computational studies to model IET

Kawatsu and Beratan have investigated IET in a generic multi-domain enzyme, in which the two domains are linked by a flexible tether, (similar to SO) and found that the entropic contribution to the donor-acceptor potential is dependent on the flexibility of the tether [31]. Pushie *et al.* examined the dynamic motion of the N-terminal and C-terminal domains and the dynamics of the active site of fully reduced cSO by molecular dynamics simulations [22]. These simulations also provided key residues that are important in IET. They include R450, D321, Y322, A186, and A297 in cSO numbering. The Y343F variant of hSO (which corresponds to Y322 in cSO) has been studied extensively, and the results indicate that Tyr-343 is involved in the binding of the substrate and that the OH group of Tyr-343 is vital for efficient IET in SO [28]. More recently, a steered molecular dynamics study of cSO by Utesch and Mroginski revealed a stable 3-dimensional “docked” structure with a short Mo... Fe distance of ~19 Å [24]. Thus, both of these molecular dynamics studies predicted that the domains of SO are highly mobile, and support the previous proposal by Feng *et al.* of domain motion in solution [8, 23, 25], and the suggestion that the tether linking the heme and the molybdenum domains might aid in this movement.

### Biochemical studies of varying the tether structure

The effect of change in the flexibility has been explored by replacing two prolines, (P105 and P111) by alanines in hSO [4–6]. The P105 residue is adjacent to the heme domain, and the P105A mutant would presumably have increased tether flexibility. However, the P105A mutant displayed a pronounced *decrease* in the IET rates while the P111A (located in the middle of the tether) showed little effect on the IET kinetics. These results suggest that the more restricted conformations of P105 favor an orientation of the heme domain that gives faster IET rates.

The effect of the tether length has been explored by shortening the tether by deleting three (KVA), four (KVAT), and five (KVATV) non-conserved amino acid residues from the tether [5, 6]. The largest decrease in the IET rate was for the five amino acid deletion mutant, and IET became the rate-limiting step in catalysis (Table 1). These results suggested that

decreasing the length of the tether can influence the conformational transition required to bring the heme and the molybdenum centers into a suitable mutual orientation.

### Human pathogenic mutants

Recently, the first successful treatment of a child with molybdenum cofactor deficiency (also known as “general sulfite oxidase deficiency”) has been demonstrated by supplying a key chemical precursor that was lacking for the complete biosynthesis of molybdopterin [2, 32]. However, no treatments are yet available for “isolated sulfite oxidase deficiency”, which is caused by certain inherited point defects in the *sox* gene (Table 2) and produces the same severe neonatal neurological symptoms [33].

Several mutations that have been associated with human SO deficiency in patients (R160Q, G473D, A208D, K322R) are in the molybdenum domain, near the active site. The R160Q mutant at the substrate binding site showed that both  $K_m$  for sulfite and  $k_{cat}$  are markedly affected, leading to a decrease in  $k_{cat}/K_m$  sulfite of roughly 3 orders of magnitude [34]. The IET kinetics has been also affected; at pH 6.0, the  $k_{et}$  value of R160Q is only  $0.64\text{ s}^{-1}$  compared to  $411\text{ s}^{-1}$  for the wild type under the same conditions. The  $k_{et}$  value of the R160K mutant only decreases about 4-fold, being intermediate in value between those of the wild type and the R160Q mutant. The marked decrease in the physiologically relevant IET process for the R160Q mutation strongly suggests that the positive charge of R160 is critical for rapid IET in humans. These results provide an experimental rationale for the fatal impact of R160Q mutant in human disease. Similar studies on G473D and A208D pathogenic mutants revealed that the IET rate constants at pH 6.0 are decreased by 3 orders of magnitude relative to that of *wt*. Steady-state kinetic measurements indicate that the IET process is the rate-limiting step in the catalytic cycle for all three of these mutants [35, 36].

Recently the biochemical and biophysical basis for the pathology of K322R in humans has been studied in our group. The K322 residue interacts with the phosphate group of the molybdopterin cofactor, and it is relatively buried in the Mo domain (Fig. 3). The steady-state parameters reveal that the catalytic efficiency ( $k_{cat}/K_m^{\text{sulfite}}$ ) for the K322R mutant is comparable to that of the *wt*, due to the similar increments (10-fold) in both  $k_{cat}$  and  $K_m^{\text{sulfite}}$ . It is important to note, however, that the Michaelis-Menten constant,  $K_m^{\text{sulfite}}$ , is increased significantly relative to the *wt* value ( $11 \pm 0.4$  for *wt* vs  $97 \pm 27\text{ }\mu\text{M}$  for K322R). At pH 8.0, the IET rate constant for K322R human SO is  $120 \pm 2\text{ s}^{-1}$  (Fig. 4) and it is smaller than the  $k_{cat}$  value at the same pH ( $201 \pm 18\text{ s}^{-1}$ ). This suggests that for the K322R mutant at pH 8.0 the IET has become the rate-limiting step for catalysis. The equilibrium constant ( $K_{eq}$ ) values for the K322R mutant at various pH values are given in Table 3. The maximum  $K_{eq}$  is observed at pH 7.4 for *wt* hSO and the mutant K322R follows the same trend. However,  $K_{eq}$  is significantly larger for K322R compared to *wt* values at all pH values studied. The large value of  $K_{eq}$  for K322R indicates that the Mo(V)/Fe(III) state is thermodynamically significantly more stabilized for the mutant than *wt* hSO. The measured heme potential is essentially unchanged, while the calculated Mo potential is shifted by about 50 mV to more positive values compared to *wt* hSO ( $+16 \pm 5\text{ mV}$  for *wt* and  $+65 \pm 3\text{ mV}$  for K322R, vs. SHE). The K322R mutation may have altered the H-bonding network among N161, D303, R160, and especially the interaction with the phosphate oxygen of the Moco group, which may have contributed to the observed positive shift in the Mo potential. The positive shift of the Mo potential can, in principle, provide conditions for stabilization of Mo(V)/Fe(III) as the resting state of the enzyme in the K322R mutant, in contrast to *wt* hSO, where the resting state is Mo(VI)/Fe(III). This hypothesis is supported by a readily detectable Mo(V) EPR signal in the continuous wave (CW) electron paramagnetic resonance (EPR) of the as-isolated K322R hSO in the phosphate storage buffer at pH 7.8. For *wt* hSO, only a very weak Mo(V) EPR signal is observed from the as-isolated enzyme. The introduction of a relatively larger guanidinium group of an Arg in place of Lys, may have

caused significant conformational changes in the Moco binding pocket. The loss or changes of some of the interactions formed by Lys may be the reason for the observed positive shift in the Mo potential. The change in the Mo potential might impair the IET step making it rate limiting in the catalysis. Another reason for a reduced IET would be the loss of the H-bonding network created by Lys322 with the nearby residues (Fig. 3). It was previously proposed that the motion of Mo and Fe centers into closer proximity generates a transient complex which may facilitate the rapid IET observed in wt hSO [8, 17, 37]. Once the redox centers are in close proximity, rapid transfer of electrons is dependent on the thermodynamic driving force (redox potentials of the donor and the acceptor) and the reorganization energy. The thermodynamic driving force in the wt hSO is approximately 40 mV. However, the driving force in the K322R mutant should be substantially smaller due to the positive shift in the Mo(VI/V) midpoint potential. As indicated by the large  $K_m^{\text{sulfite}}$ , the K322R enzyme requires the presence of a large amount of sulfite (100  $\mu\text{M}$ ) to turn over. The normal physiological concentration of sulfite is  $4.9 \pm 2.5$  (mean  $\pm$  S.D.)  $\mu\text{Mol/L}$  [38]. This also implies that this mutant is catalytically incompetent under physiological conditions, thereby rationalizing the fatal effect of the K322R mutation in human SO.

### Aromatic residues

The existing model for IET in SO involves the motion of the negatively charged cytochrome  $b_5$  domain via a flexible tether toward the cationic substrate-binding pocket of the Mo domain to reduce the Mo-Fe distance and thereby to achieve the fast IET rates observed experimentally [17]. However, the simultaneous occurrence of two processes at the active site, i.e. heme docking for IET and substrate binding/product release may be unfavorable. Therefore, a mechanism with alternative positions for heme docking and for substrate oxidation at the active site is a plausible and attractive hypothesis.

A possible model for the productive orientation of the molybdenum and heme cofactors in hSO is provided by the crystal structure of bacterial sulfite dehydrogenase (SDH) [39], a heterodimeric member of the sulfite oxidase family which contains a Mo subunit and a heme subunit that are tightly associated with one another to give a Mo-Fe distance of 16.6 Å. Laser flash photolysis experiments on wt SDH show facile IET that is independent of solution viscosity (indicating no reorientation of the heme domain) and sulfate concentration (i.e. no inhibition by anions), and two pathways have been proposed for IET in SDH from the crystal structure. One pathway involves H-bonding between the propionate groups of the heme and the conserved active site arginine (R55 in SDH; R160 in hSO). This interaction is similar to the proposal for docking of these two domains in hSO. In hSO, the R160Q mutation is fatal and disrupts both IET and steady-state catalysis. However, for SDH, the analogous R55Q mutation has no effect on IET [7]. Therefore, it was concluded that the primary role of R160 in hSO is to aid in docking the heme domain and in binding substrate. A second, alternative IET pathway in SDH proposed from the crystal structure involves the sequence of aromatic residues (Phe-168, Tyr-236, Trp-231, Phe-230, and Tyr-61) that is located between the two cofactors with edge-to-edge distances of about 4 Å [39]. It is important to note here that electron transfer could occur with tyrosine and tryptophan residues as were shown in several past studies [40–42], but evidence for electron transfer through phenylalanine or histidyl residues are unknown. Investigation of the structure of cSO shows that its molybdenum cofactor also contains a series of aromatic amino acids (Y273, W338 and H337) that are stacked against the pterin ring system, separated by interplanar spacings of  $\sim 4$  Å, and which extend to the surface of the molybdenum domain (Fig. 5). For SDH it has not yet been possible to prepare mutations of all of the aromatic residues in the alternative pathway in order to determine their effects on IET rates. Very recently, the effects of modifying this proposed alternative IET pathway in hSO was investigated by mutating Y273 (which is adjacent to the pterin ring) as well as the two

adjacent aromatic surface residues in the Mo domain, W338 and H337. These three residues in hSO correspond to residues F168, W331 and F230 in the proposed alternative aromatic IET pathway between the molybdenum cofactor and the heme of SDH.

Fig. 5 shows an electrostatic potential map and a schematic diagram of the pertinent region of the cSO structure, but with amino acid residues given the hSO numbers to facilitate the presentation and discussion of the results. The active site of SO consists of a solvent-exposed pocket lined with positively charged amino acids that facilitate the substrate binding as illustrated in Fig. 5B. Residues Y273, H337 and W338 are located away from the substrate-binding pocket, but all are within  $\sim 9$  Å of the Mo atom.

The mutations of H337 and W338 dramatically *decrease* the IET rate constant by approximately 100-fold relative to *wt* (Fig. 6), implying that their specific identities (i.e. a histidine at 337 and a tryptophan at 338) are important for rapid ET. The sharp decrease in IET associated with these mutations is also consistent with the hypothesis that these two residues create a suitable docking site away from the substrate-binding pocket, and thereby play an important role in facilitating rapid IET between Mo and the heme centers.

Redox potential measurements using spectroelectrochemistry have revealed that the mutations of these aromatic residues can also affect the potential of the heme center (Fig. 7), which is presumed to be distant based on the crystal structure of cSO. The dramatic decreases in IET rates observed for Y273A, and for the mutants of H337 and W338 in hSO also support the hypothesis, developed from the crystal structure of SDH, that these aromatic residues, which are conserved in vertebrates, form a favorable interaction site for the heme center for IET 2 (Fig. 1) in flash photolysis experiments [39].

Previous microcoulometric studies have shown that the overall thermodynamic driving force for the IET 2 reaction in SO (Fig. 1) is small [20]. The overall driving force has not been measured directly for these mutants of Fig. 6, but spectroelectrochemical studies of the Fe(III/II) couples show changes of only  $\pm 30$  mV or less. In addition, the CW-EPR spectra indicate no change in the structure of the Mo center. Therefore, it is reasonable to assume that the overall driving force in these aromatic mutants is similar to *wt*, and that the decreased IET rates may be due to several factors: a greater Mo-Fe distance, an unfavorable reorganization energy, or a slower conformational step, the latter of which may be due to the presence of a “non-productive” resting state of these mutant forms of the hSO enzyme.

### Heme mutants

Most studies of IET in hSO have focused on mutations near the molybdenum active site and of the tether linking the two domains, rather than the heme domain. As discussed previously, the idea of a mobile heme domain is supported by experimental and theoretical studies of SO [22, 24]. Therefore, it is also essential to understand the role of amino acid residues near the heme in IET kinetics. Preliminary investigations have been initiated for several mutations of amino acid residues in the heme domain of hSO. The most interesting results were observed for the mutants of His-90, which is H-bonded to the propionate oxygen of the heme. Mutating His-90 to Phe decreased the IET rate constant, while the H90Y mutant displayed a significant increase in the IET rate constants at low pH values [43].

### Summary

Animal SOs possess two redox-active domains and are ideal for studying IET in relation to the overall conformation of the protein and the molecular dynamics of the motion of the two domains relative to one another. The procedures for preparing and purifying recombinant hSO [34, 44] have been further optimized in our laboratory [4, 5, 29], so that a wide range of

mutant proteins in 50–100 mg quantities can be prepared for comprehensive kinetic, mechanistic, and spectroscopic studies. The ready accessibility of recombinant hSO has made it possible to investigate the effects of modifying amino acid residues of interest to better understand the long range IET process in hSO and to obtain insight into biochemical basis of pathological mutations of hSO.

Experimental and theoretical studies agree that domain movement is necessary for SO to achieve a productive conformation during electron transfer, and that the length and composition of the interdomain tether is an important factor in the rates of IET. However, the interactions such as hydrogen bonding and hydrophobic effects involved in mediating the correct mutual orientation and the distance following the initial orientation are unknown. Studies of site-specific mutants reveal a great deal about the IET complex in hSO. Mutating several aromatic residues that extend from the pterin to the surface of the protein suggest that alternative ET pathways may be in operation in hSO. The profound effects of mutating residues surrounding the Mo active site (e. g. R160Q and Y343F) have been demonstrated [28, 45], and extension to mutations of other positively charged residues surrounding the active site, such as Lys200, is warranted.

Finally, all of the discussions presented here and elsewhere for IET in hSO rest upon the single structure of intact native cSO. It is clear that X-ray crystal structures of hSO and various mutants are needed to better understand the unexpected properties of this fascinating biomedically important protein.

## Acknowledgments

We acknowledge support by the National Institutes of Health (Grant R01-037773 to J.H.E). We thank K. V. Rajagopalan for providing the pTG918 plasmid containing the hSO gene for preparing recombinant human sulfite oxidase and the protocols for purifying the enzyme. We are grateful to F. Ann Walker for the use of equipment and for helpful discussions. We acknowledge heme mutant studies by Amanda Davis.

## Reference

1. Rupa CA, Gillett J, Gordon BA, Ramsay DA, Johnson JL, Garrett RM, Rajagopalan KV, Jung JH, Bachevie GS, Seller AR. *Neuropediatrics*. 1996; 27:299–304. [PubMed: 9050047]
2. Schwahn BC, Galloway PG, Bowhay S, Veldman A, Santamaria JA, Schwarz G, Belaidi AA. *J. Inher. Metab. Dis*. 2010; 33:S29–S39.
3. Kisker C, Schindelin H, Pacheco A, Wehbi W, Garrett RM, Rajagopalan KV, Enemark JH, Rees DC. *Cell*. 1997; 91:973–983. [PubMed: 9428520]
4. Johnson-Winters K, Tollin G, Enemark JH. *Biochemistry*. 2010; 49:7242–7254. [PubMed: 20666399]
5. Johnson-Winters K, Nordstrom AR, Emesh S, Astashkin AV, Rajapakshe A, Berry RE, Tollin G, Enemark JH. *Biochemistry*. 2010; 49:1290–1296. [PubMed: 20063894]
6. Johnson-Winters K, Nordstrom AR, Davis AC, Tollin G, Enemark JH. *Metallomics*. 2010; 2:766–770. [PubMed: 21072368]
7. Emesh S, Rapson TD, Rajapakshe A, Kappler U, Bernhardt PV, Tollin G, Enemark JH. *Biochemistry*. 2009; 48:2156–2163. [PubMed: 19226119]
8. Feng C, Tollin G, Enemark JH. *Biochim. Biophys. Acta*. 2007; 1774:527–539. [PubMed: 17459792]
9. Feng CJ, Kappler U, Tollin G, Enemark JH. *J. Am. Chem. Soc*. 2003; 125:14696–14697. [PubMed: 14640631]
10. Rajagopalan, KV.; Johnson, JL. *Wiley Encyclopedia of Molecular Medicine*. Creighton, TE., editor. New York: Wiley; 2002. p. 3048
11. Rajagopalan, KV. *Molybdenum and Molybdenum Containing Enzymes*. Coughlan, M., editor. Pergamon; 1980. p. 243

12. Hille R. *Chem. Rev.* 1996; 96:2757–2816. [PubMed: 11848841]
13. Enemark JH, Astashkin AV, Raitsimring AM. *Dalton Trans.* 2006:3501–3514. [PubMed: 16855750]
14. Wilson HL, Wilkinson SR, Rajagopalan KV. *Biochemistry.* 2006; 45:2149–2160. [PubMed: 16475804]
15. Wilson HL, Rajagopalan KV. *J. Biol. Chem.* 2004; 279:15105–15113. [PubMed: 14729666]
16. Brody MS, Hille R. *Biochemistry.* 1999; 38:6668–6677. [PubMed: 10350486]
17. Pacheco A, Hazzard JT, Tollin G, Enemark JH. *J. Biol. Inorg. Chem.* 1999; 4:390–401. [PubMed: 10555573]
18. Marcus RA, Suttin N. *Biochim. Biophys. Acta.* 1985; 811:265–322.
19. Beratan DN, Skourtis SS, Balabin IA, Balaeff A, Keinan S, Venkatramani R, Xiao D. *Acc. Chem. Res.* 2009; 42:1669–1678. [PubMed: 19645446]
20. Spence JT, Kipke CA, Enemark JH, Sunde RH. *Inorg. Chem.* 1991; 30:3011–3015.
21. Rajapakshe A, Meyers K, Berry R, Tollin G, Enemark J. *J. Biol. Inorg. Chem.* 2012; 17:345–352. [PubMed: 22057690]
22. Pushie MJ, George GN. *J. Phys. Chem. B.* 2010; 114:3266–3275. [PubMed: 20158265]
23. Feng C, Kedia RV, Hazzard JT, Hurley JK, Tollin G, Enemark JH. *Biochemistry.* 2002; 41:5816–5821. [PubMed: 11980485]
24. Utesch T, Mroginski MA. *J. Phys. Chem. Lett.* 2010; 1:2159–2164.
25. Feng CJ, Kedia RV, Hazzard JT, Hurley JK, Tollin G, Enemark JH. *Biochemistry.* 2002; 41:5816–5821. [PubMed: 11980485]
26. Sullivan EP Jr, Hazzard JT, Tollin G, Enemark JH. *J. Am. Chem. Soc.* 1992; 114:9662–9663.
27. Sullivan EP, Hazzard JT, Tollin G, Enemark JH. *Biochemistry.* 1993; 32:12465–12470. [PubMed: 8241137]
28. Feng CJ, Wilson HL, Hurley JK, Hazzard JT, Tollin G, Rajagopalan KV, Enemark JH. *J. Biol. Chem.* 2003; 278:2913–2920. [PubMed: 12424234]
29. Rajapakshe A, Johnson-Winters K, Nordstrom AR, Meyers KT, Emesh S, Astashkin AV, Enemark JH. *Biochemistry.* 2010; 49:5154–5159. [PubMed: 20491442]
30. Kessler DL, Rajagopalan KV. *Biochim. Biophys. Acta.* 1974; 370:389–398. [PubMed: 4374240]
31. Kawatsu T, Beratan DN. *Chem. Phys.* 2006; 326:259–269.
32. Veldman A, Santamaria-Araujo JA, Sollazzo S, Pitt J, Gianello R, Yapliito-Lee J, Wong F, Ramsden CA, Reiss J, Cook I, Fairweather J, Schwarz G. *Pediatrics.* 2010; 125:E1249–E1254. [PubMed: 20385644]
33. Johnson JL, Coyne KE, Garrett RM, Zabot MT, Dorche C, Kisker C, Rajagopalan KV. *Hum. Mutat.* 2002; 20:509/501–509/506.
34. Garrett RM, Johnson JL, Graf TN, Feigenbaum A, Rajagopalan KV. *Proc. Natl. Acad. Sci. U.S.A.* 1998; 95:6394–6398. [PubMed: 9600976]
35. Feng C, Wilson HL, Tollin G, Astashkin AV, Hazzard JT, Rajagopalan KV, Enemark JH. *Biochemistry.* 2005; 44:13734–13743. [PubMed: 16229463]
36. Feng C, Wilson HL, Hurley JK, Hazzard JT, Tollin G, Rajagopalan KV, Enemark JH. *Biochemistry.* 2003; 42:12235–12242. [PubMed: 14567685]
37. Pacheco A, Hazzard JT, Enemark JH, Tollin G. *Abstr. Pap. Am. Chem. Soc.* 1997; 213 498-INOR.
38. Mitsuhashi H, Nojima Y, Tanaka T, Ueki K, Maezawa A, Yano S, Naruse T. *J. Leukocyte Biol.* 1998; 64:595–599. [PubMed: 9823763]
39. Kappler U, Bailey S. *J. Biol. Chem.* 2005; 280:24999–25007. [PubMed: 15863498]
40. Shih C, Museth AK, Abrahamsson M, Blanco-Rodriguez AM, Di Bilio AJ, Sudhamsu J, Crane BR, Ronayne KL, Towrie M, Vlcek A Jr, Richards JH, Winkler JR, Gray HB. *Science.* 2008; 320:1760–1762. [PubMed: 18583608]
41. Jovanovic SV, Harriman A, Simic MG. *J. Phys. Chem.* 1986; 90:1935–1939.
42. Wang M, Gao J, Müller P, Giese G. *Angew. Chem. Int. Ed.* 2009; 48:4232–4234.
43. Meyers, KT.; Enemark, JH.; Rajapakshe, A. Abstracts of Papers, 241st ACS National Meeting & Exposition; United States; March 27–31, 2011; Anaheim, CA. CHED-456.

44. Temple CA, Graf TN, Rajagopalan KV. Arch. Biochem. Biophys. 2000; 383:281–287. [PubMed: 11185564]
45. Feng CJ, Wilson HL, Hurley JK, Hazzard JT, Tollin G, Rajagopalan KV, Enemark JH. Biochemistry. 2003; 42:12235–12242. [PubMed: 14567685]
46. Humphrey W, Dalke A, Schulten K. J. Molec. Graphics. 1996; 14:33–36.

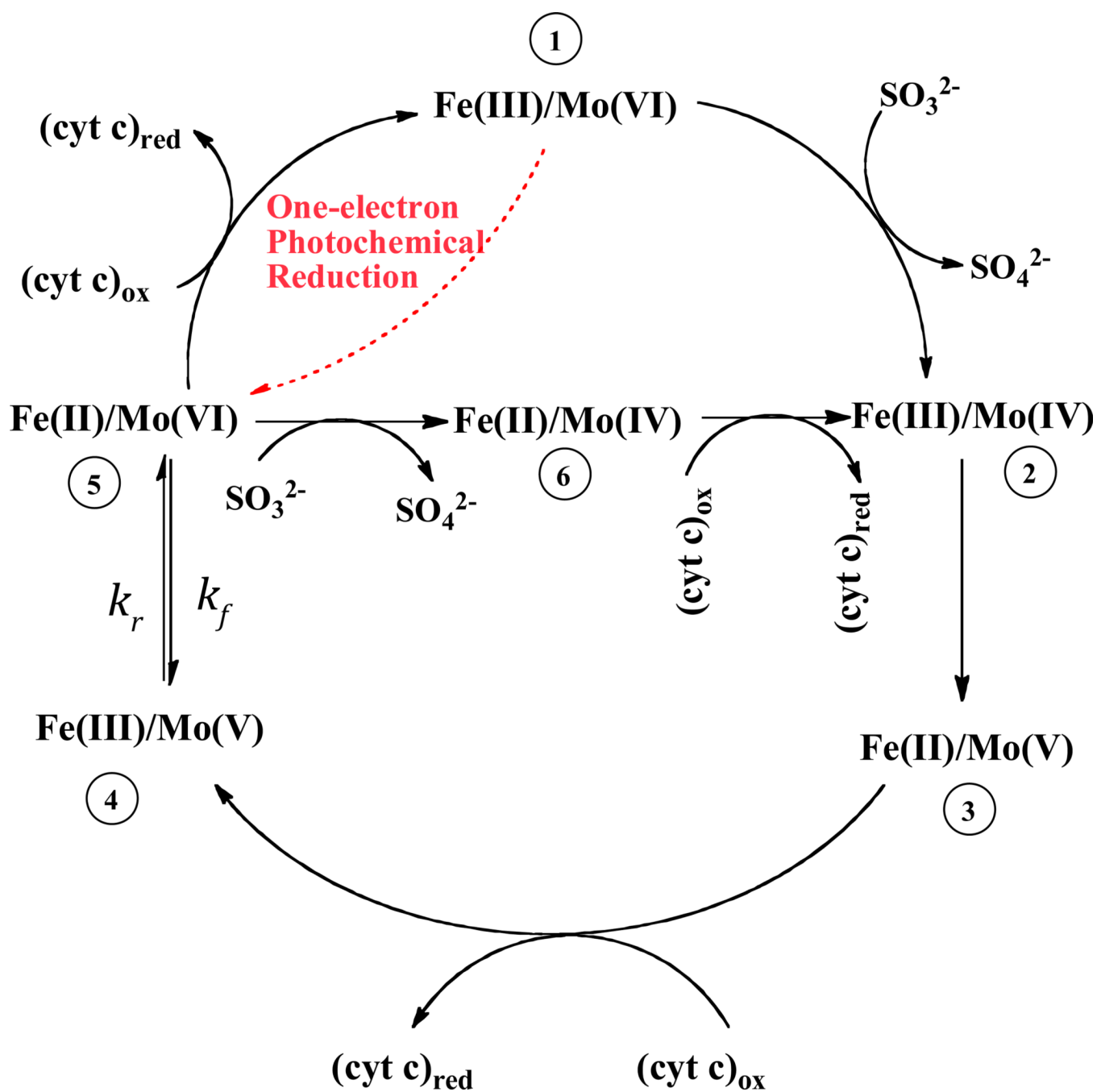


**Figure 1.**  
Proposed catalytic cycle for the oxidation of sulfite by hSO [11]

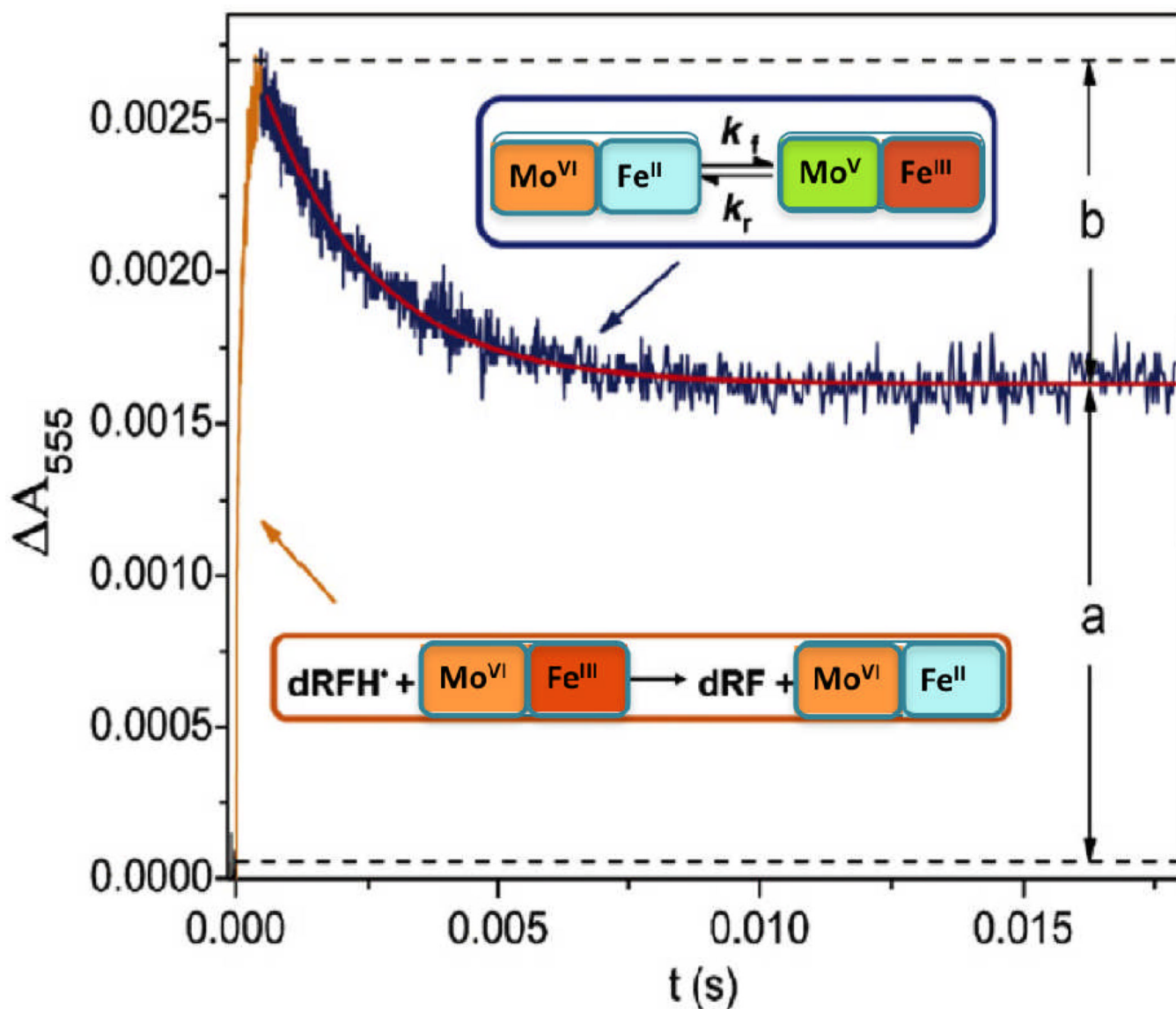


**Figure 2.** Kinetic transient obtained at 555 nm upon photoexcitation of a solution containing wild-type human SO, dRF, and 0.5 mM fresh semicarbazide hydrochloride (pH 7.4). The portion of the figure outlined by the orange box points to the initial heme reduction by dRFH $\bullet$ ; this process is pseudo-first-order, and its rate depends on protein concentration. The dark blue box points to heme reoxidation due to the subsequent IET between the Mo and Fe centers; this process is independent of protein concentration, consistent with its intraprotein nature. The red solid line indicates a single-exponential fit to the IET phase.  $K_{eq} = b/a$ . Reproduced with permission from ref [8]. Copyright 2007 Elsevier B.V.

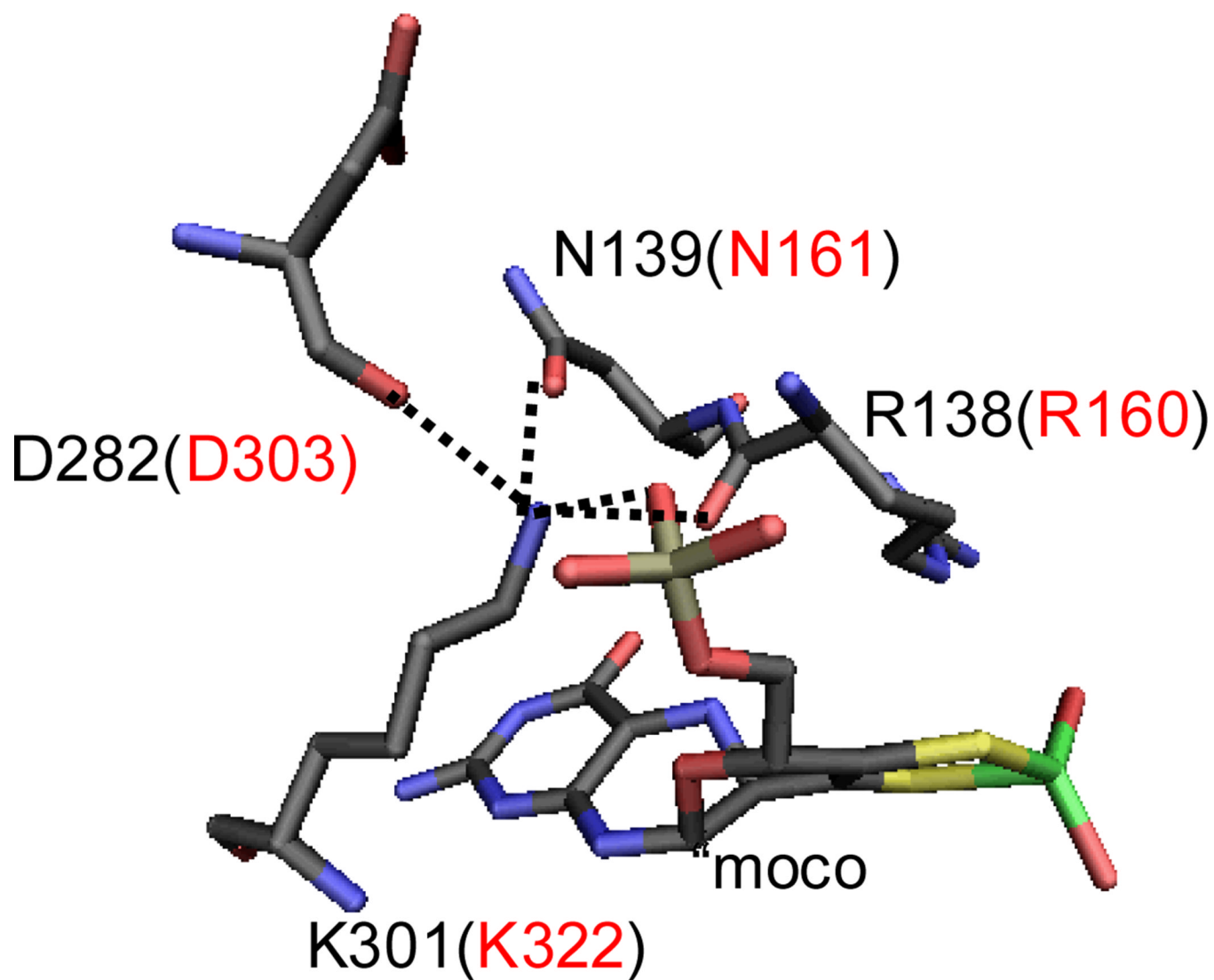


**Figure 3.**  
View into the interaction site of K322. The numbers in red are human numbering; black are chicken. The light grey is the phosphate group of Moco.

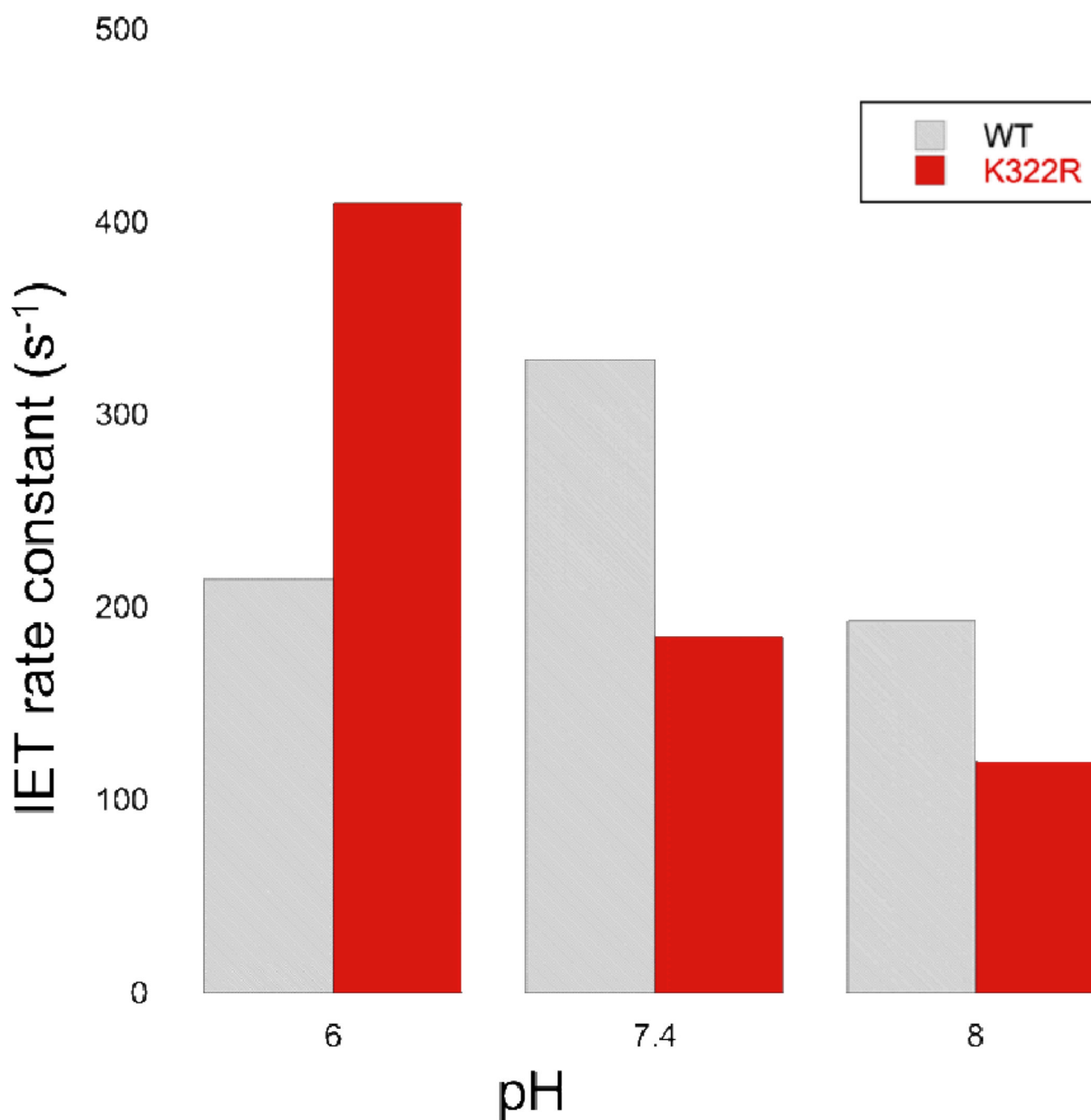


**Figure 4.**  
IET rate constants for *wt* and K322R mutant at different pH values.

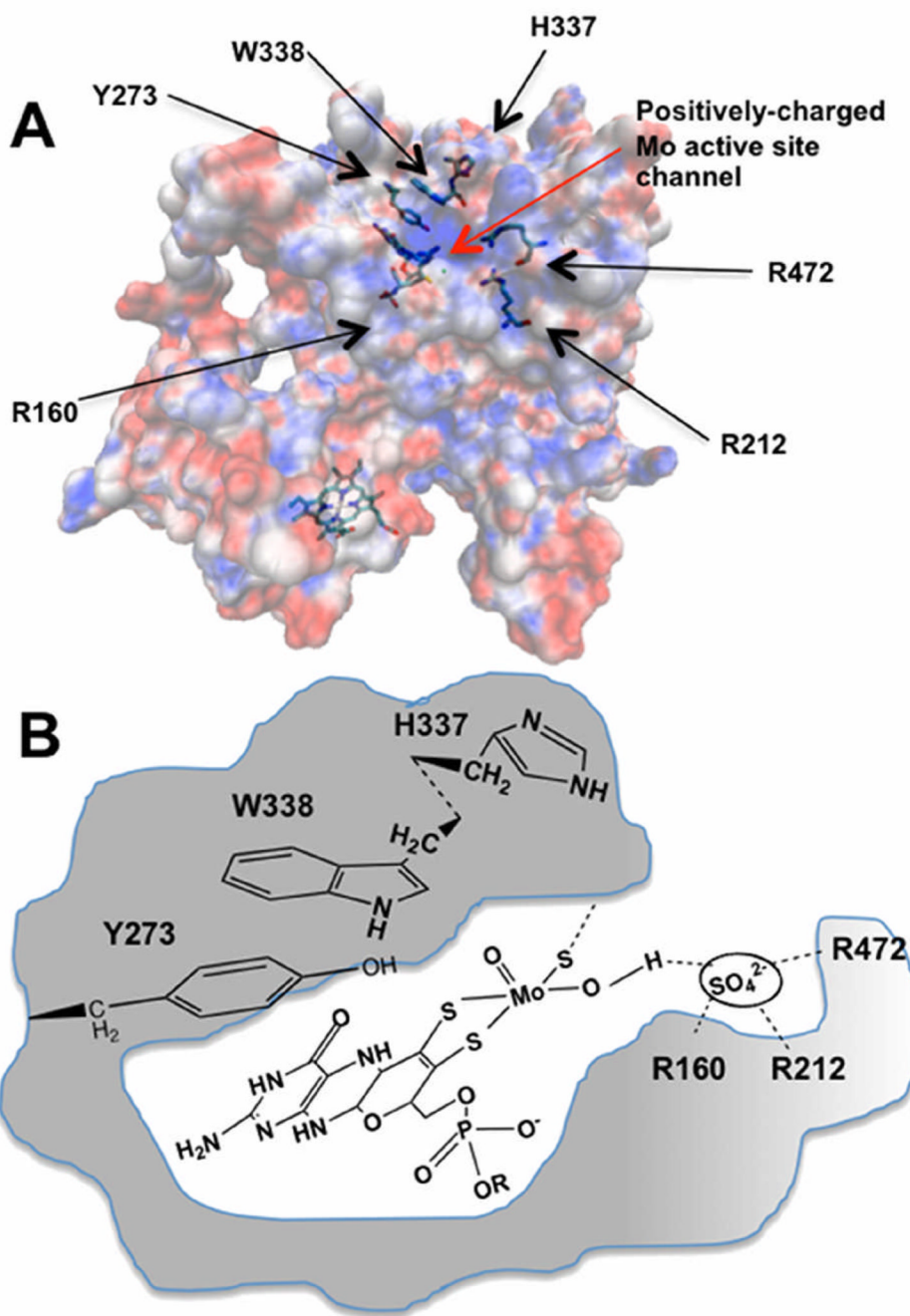


**Figure 5.**

(A) The electrostatic potential map of one of the subunits of SO contoured at color scale data range set to  $-10$  eV and  $+10$  using the VMD [46] program. The structural arrangement of Y273, W338, and H337 residues of interest in the active site of cSO is shown with residues numbered according to the hSO sequence. (B) Schematic representation of the pocket that allows access to the Mo active site from the solvent. The geometrical arrangement of W338 and H337 residues with respect to the anion-binding pocket and to the Mo active site is shown. Only the side chains of Y273, W338 and H337 are pictured. Reproduced from [21]

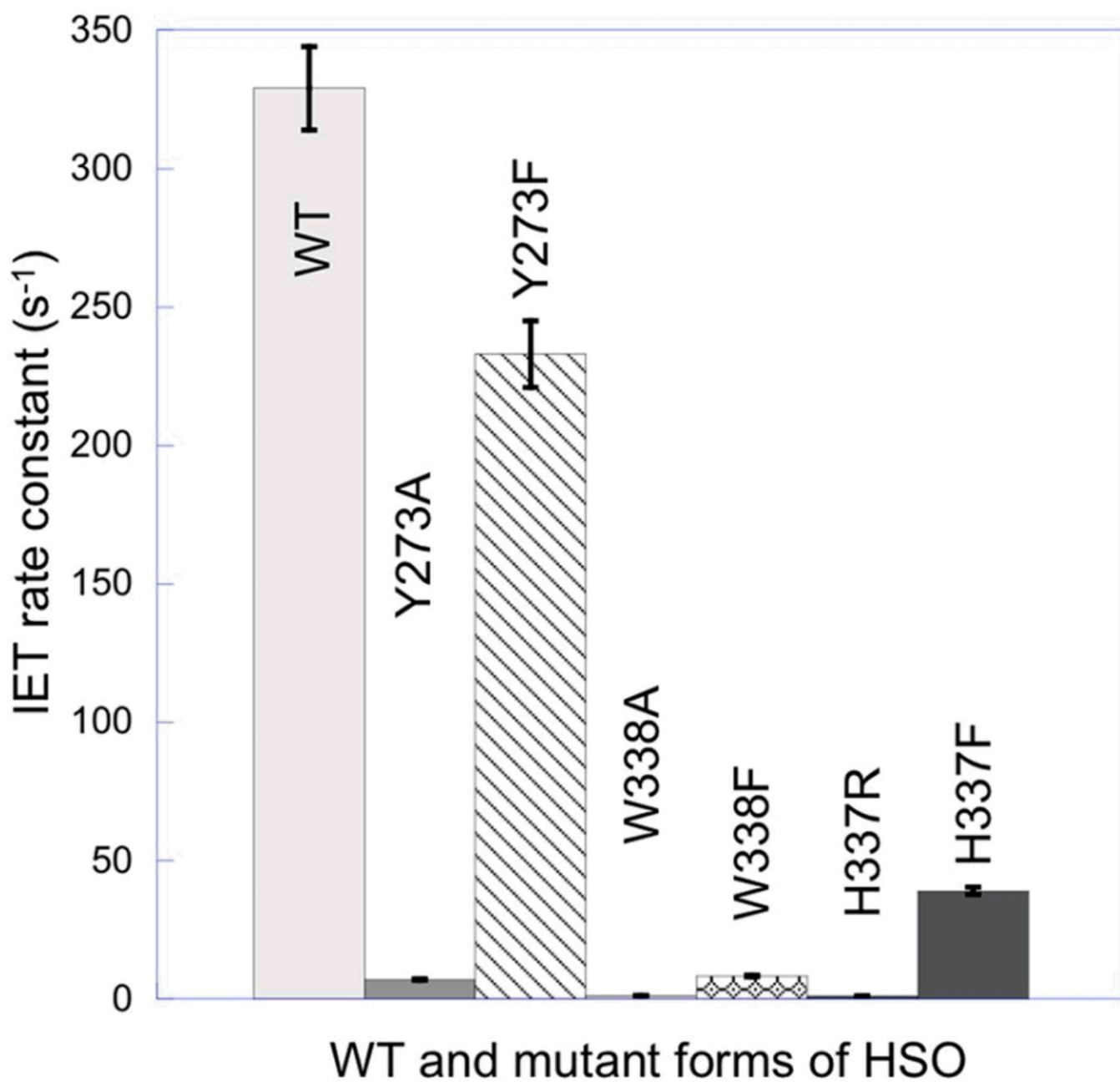


**Figure 6.**  
IET rate constants for *wt* and mutants of aromatic residues at pH 7.4.

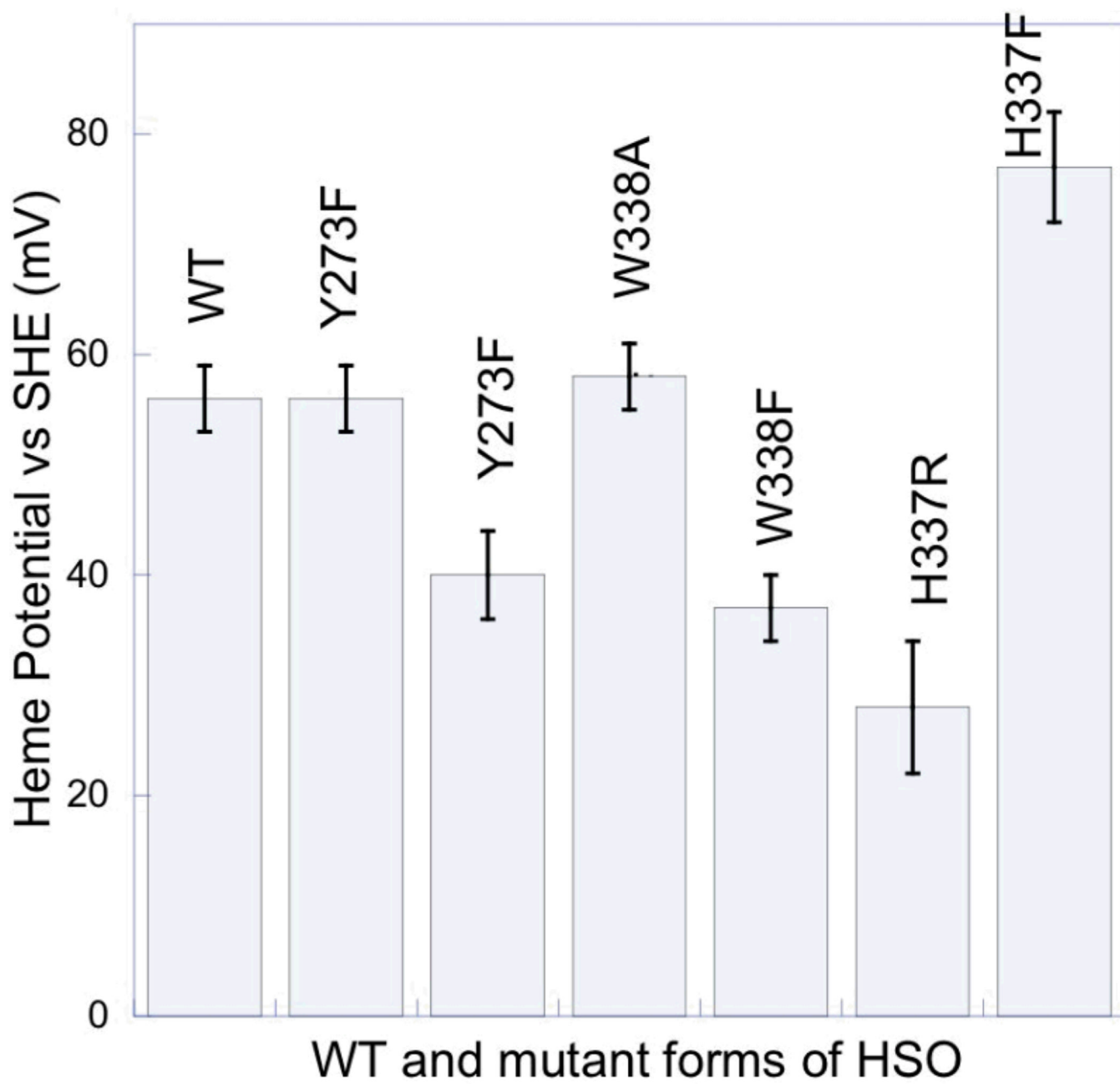


**Figure 7.** Electrochemical heme midpoint potentials for hSO and mutants at pH 7.4.

**Table 1**

IET rate constants for selected hSO mutants at pH 7.4.

| hSO Mutant     | Location  | $k_{et}$ (pH7.4) | References |
|----------------|-----------|------------------|------------|
| W338A          | Mo domain | $1.3 \pm 1$      | 21         |
| W338F          | Mo domain | $8 \pm 0.3$      | 21         |
| H337F          | Mo domain | $39 \pm 1.4$     | 21         |
| H337R          | Mo domain | $1 \pm 0.04$     | 21         |
| Y273A          | Mo domain | $7 \pm 0.8$      | 21         |
| Y273F          | Mo domain | $233 \pm 12$     | 21         |
| P111A          | tether    | $359 \pm 19$     | 5, 6       |
| P105AP111A     | tether    | $93 \pm 11$      | 5, 6       |
| P105A          | tether    | $146 \pm 23$     | 5, 6       |
| $\Delta$ KVA   | tether    | $294 \pm 14$     | 5, 6       |
| $\Delta$ KVAT  | tether    | $165 \pm 3$      | 5, 6       |
| $\Delta$ KVATV | tether    | $6.4 \pm 0.1$    | 5, 6       |

**Table 2**

Mutations identified from patients suffering from isolated sulfite oxidase deficiency [33]. Mutations in red are associated with the Mo domain; those in black are associated with the dimerization domain or with the dimerization interface.

| Base change      | Amino acid change in hSO | Amino acid change in cSO |
|------------------|--------------------------|--------------------------|
| 1. g479a         | R160Q                    | R138Q                    |
| 2. g1418a        | G473D                    | G451G                    |
| 3. g632a         | R211Q                    | R189Q                    |
| 4. c623a         | A208D                    | A186D                    |
| 5. 1016g         | Q339R                    | Q318R                    |
| 6. g1109a c1110a | S370Y                    | S349Y                    |
| 7. t1177c        | W393R                    | W372R                    |
| 8. a601c         | I201L                    | V179L                    |
| 9. g926a         | R309H                    | R288H                    |
| 10. a965g        | K322R                    | K301R                    |
| 11. g913a        | G305S                    | G284S                    |

**Table 3**

Laser flash photolysis equilibrium constants for K322R mutant at different pH values.

| Enzyme        | pH 6.0      | pH 7.4      | pH 8.0      |
|---------------|-------------|-------------|-------------|
| <i>wt</i> hSO | 0.49 ± 0.09 | 0.63 ± 0.10 | 0.46 ± 0.11 |
| K322R         | 1.22 ± 0.02 | 1.56 ± 0.01 | 1.31 ± 0.01 |